

International Journal of Modern Physics A
 © World Scientific Publishing Company

Effect of an Expanding Charged Cloud on two-particle Bose-Einstein Correlations

Hemida H. Mohammed^{1,2}, Máté Csanád³, Y. Mohammed^{1,2}, N. Rashed¹, Dániel Kincses³, M. A. Mahmoud^{1,2}

¹ *Physics Department, Fayoum University, El-Fayoum, 63514, Egypt*

² *Center for High Energy Physics (CHEP-FU), Fayoum University, El-Fayoum, 63514, Egypt*

³ *ELTE Eötvös Loránd University, Pázmány P. s. 1/a, 1117 Budapest, Hungary*

Received Day Month Year

Revised Day Month Year

In high-energy physics, quantum statistical correlation measurements are very important for getting a good picture of how a particle-emitting source is structured in space and time, as well as its thermodynamic properties and inner dynamics. It is necessary to take into account the various final state effects since they have the potential to alter the observed femtoscopic correlation functions. Protons are affected mostly by the strong interaction, whereas other charged particles are mostly influenced by the Coulomb interaction. The interaction of the particles under investigation with the fireball or the expanding cloud of the other particles in the final state might also have significant consequences. This may cause the particles' trajectory to shift. This phenomenon can be viewed as an Aharonov-Bohm effect since the pair's alternate tracks reveal a closed loop with an internal field. We investigate a numerical solution for a toy model to study the modifications of Bose-Einstein correlation function strength, which is sensitive to this effect.

Keywords: Aharonov-Bohm effect; Femtoscopy; Bose-Einstein Correlations; Quark-Gluon Plasma.

PACS numbers:

1. Introduction

After hadronization in heavy-ion collisions, a high multiplicity of pions,¹ kaons, and other charged particles are produced. The phenomenon of correlated particles can arise from several physical processes, e.g., jets, collective flow, conservation laws, and resonance decays. Another important source of correlation can be the Bose-Einstein² or Hanbury-Brown-Twiss (HBT)^{3,4} effect, where correlation functions are used to discover the geometry of the emitting source. In the case of two identically charged pions, these correlations are the major source of the momentum correlations owing to the indistinguishability of the two identical pions and their symmetrical pair wave functions. Technically, several experimental effects have to be considered that could modify the correlation functions.⁵ The space-time geometry of the particle emitting source^{6–10} may be explored by measuring Bose-Einstein correlation functions of

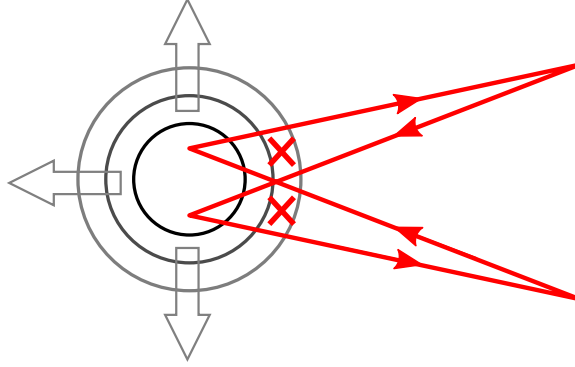


Fig. 1. Aharonov–Bohm effect with a Hubble expanding source

identical particles. In addition to quantum statistics, multiple phenomena affect the measured momentum correlations of the identical pair, the most significant being the final-state interactions.^{11,12} A further modification to the momentum correlations is due to an important effect of the interaction between any given pair of identical hadrons and the surrounding charged particles (gas cloud of charged particles) due to the potential of the charged particles in the absence of the EM field which could be interpreted as an Aharonov–Bohm like effect.^{13,14} The pair wave function experiences a phase-shift proportionate to the flux encircled by the path due to the (electromagnetic, strong, etc.) fields inside this closed path.^{14–16} The influence of the quantum-statistical correlations is modified by the phase shift, as will be covered later. We show in this work, how this phenomenon may be used in heavy-ion experiments.¹⁴

This paper is structured as follows. It starts with an introduction about Bose-Einstein correlations in high-energy physics in Section 2. In Section 3 the role of randomly fluctuating fields in multiparticle correlations is discussed. Then, in Section 4 numerical calculations are set up with a toy model to give quantitative details on how such final-state effects affect the Bose-Einstein correlation functions. Finally, in Section 5 an observable sensitive to this effect is presented, followed by conclusions.

2. Bose-Einstein correlations in relativistic collisions

In general, the two-particle momentum correlation function is defined as

$$C_2(p_1, p_2) \equiv \frac{N_2(p_1, p_2)}{N_1(p_1)N_1(p_2)}, \quad (1)$$

where $N_2(p_1, p_2)$ and $N_1(p)$ are the two- and one-particle invariant momentum distributions, with p_i being the (four-)momenta of the bosons. The pair wave function of charged bosons is a plane wave by ignoring final-state interactions. This allows the correlation function to be expressed using the phase-space density of the

particle-emitting source $S(x, p)$ as

$$C_2(p_1, p_2) = 1 + \text{Re} \frac{\tilde{S}(q, p_1) \tilde{S}^*(q, p_2)}{\tilde{S}(0, p_1) \tilde{S}^*(0, p_2)}, \quad (2)$$

where $q \equiv p_1 - p_2$ is the relative momentum, complex conjugation is denoted by $*$, and $\tilde{S}(q, p)$ denotes the Fourier transform of the source:

$$\tilde{S}(q, p) \equiv \int S(x, p) e^{iqx} d^4x. \quad (3)$$

For source functions and typical kinematic domains encountered in correlation measurements in heavy-ion collisions, the dependence of $\tilde{S}(q, p)$ as defined in Eq. (3) is much smoother in the original p momentum variable than in the relative momentum q coming from the Fourier transform, so it is customary to substitute p_1 and p_2 in Eq. (2) with an average value of $K \equiv \frac{1}{2}(p_1 + p_2)$. Hence if $p_1 \approx p_2 \approx K$, Eq. (2) gives the usual formula of

$$C_2(q, K) = 1 + \frac{|\tilde{S}(q, K)|^2}{|\tilde{S}(0, K)|^2}. \quad (4)$$

Here the dependence on the pair momentum K is smoother than on q , hence one usually thinks of q as the “main” kinematic variable, and by some parametrization for the q dependence, one explores the K dependence of the parameters of this parametric function. It is important to note furthermore, that while the above is only true for non-interacting bosons, final state interactions such as the Coulomb interaction can be handled in a simple and effective manner, outlined e.g. in Ref.^{17, 18} This usually involves the definition of a “Coulomb-correction” that removes the effect of the Coulomb interaction, and the corrected correlation functions can be analyzed then according to Eq. (4).

From Eq. (4) it is clear that the correlation function takes the value 2 at zero relative momentum. However, experimentally $C_2(0) = 1 + \lambda_2$, where λ_2 is the so-called intercept parameter (or the strength of the correlation function), and usually $\lambda_2 \leq 1$ holds. The formula for the correlation function then may be empirically modified as

$$C_2(q, K) = 1 + \lambda_2 \frac{|\tilde{S}(q, K)|^2}{|\tilde{S}(0, K)|^2}. \quad (5)$$

The reason for $\lambda_2 < 1$ can be coherent pion (or kaon) production,¹⁹ but for pions, a simpler explanation is provided by the core-halo model.² This treats the source as a sum of two components. One is the *core*: the primordial pion source, which is the main reaction zone produced in a heavy-ion collision, whose Fourier transform is resolvable in momentum (q -)space by the correlation measurement. The other component is a much wider *halo*, the contribution of the pions that are decay products of long-lived resonances (that travel much farther than $\simeq 10$ fm: η , η' , ω , K_S^0 , etc). The Fourier transform of the broad halo would be a very sharp peak at $q = 0$, and

this is experimentally essentially unresolvable. The intercept λ_2 , i.e. the extrapolation of the measured *visible* correlation function to zero relative momentum) is then basically the square of the fraction f_c of pions coming from the core (since both pions have to come from the core if they are to contribute to the visible correlation function). For the details see Ref.² So in the core-halo picture

$$\lambda_2 = f_c^2, \quad f_c = \frac{N_{core}}{N_{core} + N_{halo}}. \quad (6)$$

Hence λ_2 , the strength of the two-particle correlation measures the fraction of primordial pions. This leads to an interesting application. It is known²⁰ that in case of chiral $U_A(1)$ symmetry restoration the mass of the η' boson (the ninth, would-be Goldstone boson) is decreased, thus its production cross section is heavily enhanced. The η' has a decay channel into five pions, thus its enhancement changes λ_2 , the strength of two-pion correlation functions at low pair momentum K .²¹ This underlines the importance of understanding the effects that affect the measured λ_2 and its pair momentum dependence.

The possible presence of partially coherent pion production distorts the above picture.^{15,22,23} It turns out however, that two- and three-particle Bose-Einstein correlation functions at zero relative momentum are in simple connection to the partially coherent fraction (p_c) of the fireball:¹⁵

$$\lambda_2 = f_c^2((1 - p_c)^2 + 2p_c(1 - p_c)) \quad (7)$$

$$\lambda_3 = 2f_c^3((1 - p_c)^3 + 3p_c(1 - p_c)^2) + 3f_c^2((1 - p_c)^2 + 2p_c(1 - p_c)) \quad (8)$$

This means that a simultaneous measurement of λ_2 and λ_3 in two- and three-pion correlation functions offers the possibility of investigation of coherent pion production, in addition to the resonance decay contribution.

3. Strength of multi-particle Bose-Einstein correlations

Let us have a scenario with two point like sources, a and b , at a distance of R , emitting particles with wave functions $\Phi_a(r)$ and $\Phi_b(r)$. Let us furthermore have two detectors, A and B , separated by d , and at an L distance from the sources, with $d, R \ll L$. These detectors measure the total single particle densities at their respective locations, $\Psi(r_A)$ and $\Psi(r_B)$. We may however also measure the two-particle coinciding density $\Psi(r_A, r_B)$ i.e. the correlation function in detectors A and B :

$$C_{AB} = \frac{\langle |\Psi(r_A, r_B)|^2 \rangle}{\langle |\Phi(r_A)|^2 \rangle \langle |\Phi(r_B)|^2 \rangle} \quad (9)$$

In this section we shall discuss how this correlation function looks like for thermally emitted particles, with a random field.

3.1. Two-boson correlations with thermal emission

Let the previously mentioned sources emit bosons with wavenumber k . Then the emitted matter-waves will have the form

$$\Phi_a(r) = \frac{1}{|r - r_a|} e^{ik|r - r_a| + i\phi_a}, \quad (10)$$

$$\Phi_b(r) = \frac{1}{|r - r_b|} e^{ik|r - r_b| + i\phi_b}, \quad (11)$$

where $\phi_{a,b}$ are the (random) phases of the waves emitted from each point, while k is the wavenumber of both waves. These particles are detected in detectors A and B , where the two-particle wave-function is then

$$\begin{aligned} \Psi(r_A, r_B) &= \frac{1}{\sqrt{2}} (\Phi_a(r_A)\Phi_b(r_B) + \Phi_a(r_B)\Phi_b(r_A)) \\ &= \frac{1}{\sqrt{2}} \left(\frac{1}{|r_A - r_a||r_B - r_b|} e^{ik|r_A - r_a| + ik|r_B - r_b| + i(\phi_a + \phi_b)} \right. \\ &\quad \left. + \frac{1}{|r_B - r_a||r_A - r_b|} e^{ik|r_B - r_a| + ik|r_A - r_b| + i(\phi_a + \phi_b)} \right) \end{aligned} \quad (12)$$

The time-averaged single- and two-particle densities in detectors A and B are then (based on the uniformly distributed random thermal phases) in an approximation where $d, R \ll L$ (and defining $r_{aA} = |r_A - r_a|$ and similarly for b and B):

$$\langle |\Phi(r_{A,B})|^2 \rangle = \frac{1}{L^2} \quad (13)$$

$$\begin{aligned} \langle |\Psi(r_A, r_B)|^2 \rangle &= \frac{1}{2L^4} \left(2 + e^{ik(r_{aA} + r_{bB} - r_{aB} - r_{bA})} + e^{-ik(r_{aA} + r_{bB} - r_{aB} - r_{bA})} \right) \\ &= \frac{1}{L^4} \left(1 + \cos \left(k \frac{Rd}{L} \right) \right) \end{aligned} \quad (14)$$

as the phase average of factors like $e^{i(\phi_b - \phi_a)}$ is zero. We may observe that d/L is the angle between the two detectors, i.e. between the momenta of the pair, thus $\frac{kd}{L} = \Delta k$, the momentum difference of the pair. Then for the correlation function, one gets

$$\frac{\langle |\Psi(r_A, r_B)|^2 \rangle}{\langle |\Phi(r_A)|^2 \rangle \langle |\Phi(r_B)|^2 \rangle} - 1 = \cos \frac{kRd}{L} = \cos(R\Delta k) \quad (15)$$

At zero relative momentum, the correlation strength is then

$$\left. \frac{\langle |\Psi(r_A, r_B)|^2 \rangle}{\langle |\Phi(r_A)|^2 \rangle \langle |\Phi(r_B)|^2 \rangle} \right|_{\Delta k=0} - 1 = 1 \quad (16)$$

3.2. Effect of a random field on two-boson correlations

If random phases have to be applied not just to the points of emittance, but also to the path, then the wave functions are:

$$\Phi_a(r) = \frac{1}{|r - r_a|} e^{ik|r - r_a| + i\phi_a + i\phi(\text{path to } r)} \quad (17)$$

$$\Phi_b(r) = \frac{1}{|r - r_b|} e^{ik|r - r_b| + i\phi_b + i\phi(\text{path to } r)} \quad (18)$$

The two-particle wave-function is then

$$\begin{aligned} \Psi(r_A, r_B) &= \frac{1}{\sqrt{2}} (\Phi_a(r_A)\Phi_b(r_B) + \Phi_a(r_B)\Phi_b(r_A)) \\ &= \frac{1}{\sqrt{2}} \left(\frac{1}{r_{aA}r_{bB}} e^{ikr_{aA} + ikr_{bB} + i(\phi_a + \phi_b) + i(\phi_{aA} + \phi_{bB})} \right. \\ &\quad \left. + \frac{1}{r_{bA}r_{aB}} e^{ikr_{aB} + ikr_{bA} + i(\phi_a + \phi_b) + i(\phi_{aB} + \phi_{bA})} \right) \end{aligned} \quad (19)$$

One can again form the phase- or time-average of the single- and two-particle density in detectors A and B , in an approximation where $d, R \ll L$:

$$\langle |\Phi(r_{A,B})|^2 \rangle = \frac{1}{L^2} \quad (20)$$

$$\begin{aligned} \langle |\Psi(r_A, r_B)|^2 \rangle &= \frac{1}{2L^4} \left(2 + e^{ik(r_{aA} + r_{bB} - r_{aB} - r_{bA}) + i(\phi_{aA} + \phi_{bB} - \phi_{aB} - \phi_{bA})} \right. \\ &\quad \left. + e^{-ik(r_{aA} + r_{bB} - r_{aB} - r_{bA}) - i(\phi_{aA} + \phi_{bB} - \phi_{aB} - \phi_{bA})} \right) \\ &= \frac{1}{L^4} \left(1 + \cos \left(k \frac{Rd}{L} + \phi \right) \right) \end{aligned} \quad (21)$$

where ϕ is the total phase picked up through the random route. Normalized by the single-particle densities, one gets

$$\frac{\langle |\Psi(r_A, r_B)|^2 \rangle}{\langle |\Phi(r_A)|^2 \rangle \langle |\Phi(r_B)|^2 \rangle} - 1 = \cos \left(\frac{kRd}{L} + \phi \right) = 1 + \cos(R\Delta k + \phi) \quad (22)$$

and thus averaged over a Gaussian distribution of ϕ values, one gets

$$\frac{\langle |\Psi(r_A, r_B)|^2 \rangle}{\langle |\Phi(r_A)|^2 \rangle \langle |\Phi(r_B)|^2 \rangle} - 1 = \cos(R\Delta k) e^{-\frac{\sigma^2}{2}} \quad (23)$$

At zero relative momentum, the correlation strength is then

$$\left. \frac{\langle |\Psi(r_A, r_B)|^2 \rangle}{\langle |\Phi(r_A)|^2 \rangle \langle |\Phi(r_B)|^2 \rangle} \right|_{\Delta k=0} - 1 = e^{-\frac{\sigma^2}{2}} \quad (24)$$

3.3. Three-boson correlations with thermal emission

Let us now again turn to three-particle correlations. In this case, the three-particle symmetrized wave function is

$$\begin{aligned}\Psi(r_A, r_B, r_C) = & \frac{1}{\sqrt{6}}(\Phi_a(r_A)\Phi_b(r_B)\Phi_c(r_C) + \Phi_a(r_B)\Phi_b(r_C)\Phi_c(r_A) + \\ & \Phi_a(r_C)\Phi_b(r_A)\Phi_c(r_B) + \Phi_a(r_C)\Phi_b(r_B)\Phi_c(r_A) + \Phi_a(r_A)\Phi_b(r_C)\Phi_c(r_B) \\ & + \Phi_a(r_B)\Phi_b(r_A)\Phi_c(r_C)) = \frac{1}{\sqrt{6}L^3}e^{i(\phi_a+\phi_b+\phi_c)}(e^{ik(r_{aA}+r_{bB}+r_{cC})} \\ & + e^{ik(r_{aB}+r_{bC}+r_{cA})} + e^{ik(r_{aC}+r_{bA}+r_{cB})} + e^{ik(r_{aC}+r_{bB}+r_{cA})} \\ & + e^{ik(r_{aA}+r_{bC}+r_{cB})} + e^{ik(r_{aB}+r_{bA}+r_{cC})})\end{aligned}\quad (25)$$

where the factor $\exp i(\phi_a + \phi_b + \phi_c)$ is contained in each term. Then the phase-averaged three-particle density is:

$$\langle |\Psi(r_A, r_B, r_C)|^2 \rangle = \frac{1}{6L^6} (6 + (30 \text{ other cross-terms})) \quad (26)$$

we refrain here from writing all of them out, but point out that at zero relative momenta all terms become unity at, thus

$$\frac{\langle |\Psi(r_A, r_B, r_C)|^2 \rangle}{\langle |\Phi(r_A)|^2 \rangle \langle |\Phi(r_B)|^2 \rangle \langle |\Phi(r_C)|^2 \rangle} \Big|_{\Delta k=0} - 1 = 5 \quad (27)$$

Note that here $k\Delta r$ type of terms were converted to $R\Delta k$. This is possible due to geometrical symmetry, as discussed in the first sections.

3.4. Effect of a random field on three-boson correlations

If there are random fields picked up in different paths, then these enter in the tree-particle wave function as

$$\begin{aligned}\Psi(r_A, r_B, r_C) = & \frac{1}{\sqrt{6}L^3}e^{i(\phi_a+\phi_b+\phi_c)} \\ & \times \left(e^{ik(r_{aA}+r_{bB}+r_{cC})+i(\phi_{aA}+\phi_{bB}+\phi_{cC})} + e^{ik(r_{aB}+r_{bC}+r_{cA})+i(\phi_{aB}+\phi_{bC}+\phi_{cA})} \right. \\ & + e^{ik(r_{aC}+r_{bA}+r_{cB})+i(\phi_{aC}+\phi_{bA}+\phi_{cB})} + e^{ik(r_{aC}+r_{bB}+r_{cA})+i(\phi_{aC}+\phi_{bB}+\phi_{cA})} \\ & \left. + e^{ik(r_{aA}+r_{bC}+r_{cB})+i(\phi_{aA}+\phi_{bC}+\phi_{cB})} + e^{ik(r_{aB}+r_{bA}+r_{cC})+i(\phi_{aB}+\phi_{bA}+\phi_{cC})} \right) \quad (28)\end{aligned}$$

and from this, we have to calculate $\langle |\Psi(r_A, r_B, r_C)|^2 \rangle$ again. We can observe that in this case there will be three type of terms:

- 6 terms like $|e^{ik(r_{aA}+r_{bB}+r_{cC})+i(\phi_{aA}+\phi_{bB}+\phi_{cC})}|^2 = 1$
- 6 terms where e.g. $r_{aA} + r_{bB} + r_{cC}$ meets $r_{aB} + r_{bA} + r_{cC}$, and in this case, the result is a pair-correlation type of term, i.e. $e^{ik(r_{aA}+r_{bB}-r_{aB}-r_{bA})+i(\phi_{aA}+\phi_{bB}-\phi_{aB}-\phi_{bA})}$; we get all 3 such terms and their complex conjugates as well

8 *Hemida.H.Mohammed*

- 12 “almost” pair-correlation like terms, where e.g. $r_{aB} + r_{bC} + r_{cA}$ that meets $r_{aB} + r_{bA} + r_{cC}$; in this case, the result is $e^{ik(r_{bC}+r_{cA}-r_{bA}-r_{bA})+i(\phi_{bC}+\phi_{cA}-\phi_{aB}-\phi_{cC})}$; these don’t represent closed loops, but contain only four paths.
- 12 terms containing nine paths i.e. nine $i\phi_{xX}$ like terms in the exponent

all these get different weights when averaged on all the ϕ_{xX} phases.

Now, let us try to estimate the value of the correlation function at zero relative momenta. Previously, we introduced a single phase ϕ as a sum of four ϕ_{xX} like phases, and this was supposed to have a Gaussian distribution of $\exp -\phi^2/(2\sigma^2)$. Based on the summing of random variables, this means that a single ϕ_{xX} like phase has to have the distribution of $\exp -\phi^2/(2(2\sigma)^2)$, i.e. a double width of 2σ . Henceforth the terms that contain a sum of four paths and four phases in the exponent will again have a distribution of $\exp -\phi^2/(2\sigma^2)$, while the terms with nine paths will have a multiplier of $\exp -\phi^2/(2(2\sigma/3)^2)$. In the end, the result will be

$$\left. \frac{\langle |\Psi(r_A, r_B, r_C)|^2 \rangle}{\langle |\Phi(r_A)|^2 \rangle \langle |\Phi(r_B)|^2 \rangle \langle |\Phi(r_C)|^2 \rangle} \right|_{\Delta k=0} - 1 = \frac{1}{6} \left(6 + 18e^{-\frac{\sigma^2}{2}} + 12e^{-\frac{(2\sigma/3)^2}{2}} \right) - 1 = 3e^{-\frac{\sigma^2}{2}} + 2e^{-\frac{2\sigma^2}{9}} \quad (29)$$

4. Toy model and calculations

After rehadronization in heavy-ion collisions, hundreds of charged particles are produced. When measuring the correlation functions, we take into account that the produced hadrons create a strong electromagnetic field around trajectories of the investigated pairs of identical pions. Although this may be seen as an Aharonov-Bohm effect, a more straightforward explanation would be that the phase along the pair’s closed path is altered when one of the particles’ paths is altered by a phase, as compared to the interaction-free case, when the path is a straight line, and momentum also does not change. This additional phase shift for an infinitesimal path element dx can be expressed as $k \cdot dx$, where $k = p/\hbar$ is the momentum (or wavenumber) of the particle at that point. The alteration of the particles’ flight time reaching the detector can be connected to the phase shift of the particles, as we discuss below.

The model we set up describes the path of the particles from the collision point to the detector based on equations (30)-(31). We calculate the phase shift by taking into account the Aharonov-Bohm-like effect in form of the Coulomb interaction between the probe particles with charged particles of the cloud. This cannot be solved analytically, so we apply a numerical calculation, as detailed below. The N_{ch} produced charged particles are normally distributed (Gaussian distribution) with zero total charge and with fireball radius R , undergoing 3D Hubble flow which describes the time evolution of the produced hadron gas of charged particles after the freeze-out process. Thus for the location vector \mathbf{r} of the fireball particles, we

follow a simple time-dependence determined by $\dot{\mathbf{r}}(t) = H(t) \cdot \mathbf{r}(t)$, where $H(t) = 1/t$ is the Hubble-constant (constant in space, but inversely proportional to time). We then follow the movement of a charged probe particle, affected by all the particles of the charged cloud (without backreaction). We prepared the simulation code in C++ using the Euler method with time iteration, tracking the movement of a pion with mass $m \approx 139.57$ MeV (utilizing $c = 1$ units), from an initial location characterized by a distance d from the origin. There are several simulated scenarios with initial momentum in the range of $10 - 300$ MeV (again in $c = 1$ units), and tracked distances from 100 fm to 50000 fm (when the simulation is terminated and accumulated time-difference and the resulting phase-shift is calculated). Then the dynamical equations of the system are the following:

$$\frac{d\mathbf{p}}{dt} = \hbar c \alpha \sum_{j=1}^{N_{ch}} \frac{q(\mathbf{r}_j - \mathbf{X})}{r^3}, \quad (30)$$

$$\frac{d\mathbf{X}}{dt} = \mathbf{V} = \frac{\mathbf{p}}{m\gamma} \quad (31)$$

where

- \mathbf{X} is the position of the probe particle,
- \mathbf{r}_j denotes the position of the charged particles of the cloud, updated in time via the above mentioned equation ($\dot{\mathbf{r}}_j = H \cdot \mathbf{r}_j$),
- $q = \pm 1$ is the pion charge (in units of the elementary charge),
- $\hbar c \alpha \approx \frac{197.326}{137.036}$ MeV fm,
- $r = \sqrt{(\mathbf{r}_j - \mathbf{X})^2}$,
- $\gamma = \sqrt{1 - \frac{\mathbf{p}^2}{m^2}}$ is the Lorentz-factor,
- \mathbf{p} is the momentum of the pion,
- $m \approx 139.57$ MeV is the pion mass (using the natural units $c=1$),
- and the summation $j = 1 \dots N_{ch}$ goes over cloud particles.

From the numerical solution of that model, we get an example of a particle trajectory inside the potential of the charged cloud when considering the final state effects as an Aharonov-Bohm effect is shown in fig.(2) with initial transverse momentum $p_z = 300$ MeV.

In this model, we can measure the $t_{\text{TOF}}(d)$ time that is needed by the particle to travel a distance d . If $N_{ch} = 0$ (free case), then (in $c = 1$ units)

$$t_{\text{TOF}}^{(0)}(d) = d \sqrt{1 + \frac{m^2}{p^2}}. \quad (32)$$

If $N_{ch} > 0$, the particle is (relativistically) accelerated and decelerated by the same- and opposite-sign charged particles of the cloud, respectively. We studied fluctuating charge clouds (with variable N_{ch} , R and d values), from which Gaussian distributions of $\Delta t = t_{\text{TOF}}(d) - t_{\text{TOF}}^{(0)}(d)$ emerged, with a width σ_t depending on initial momentum p_t of the probe particle.

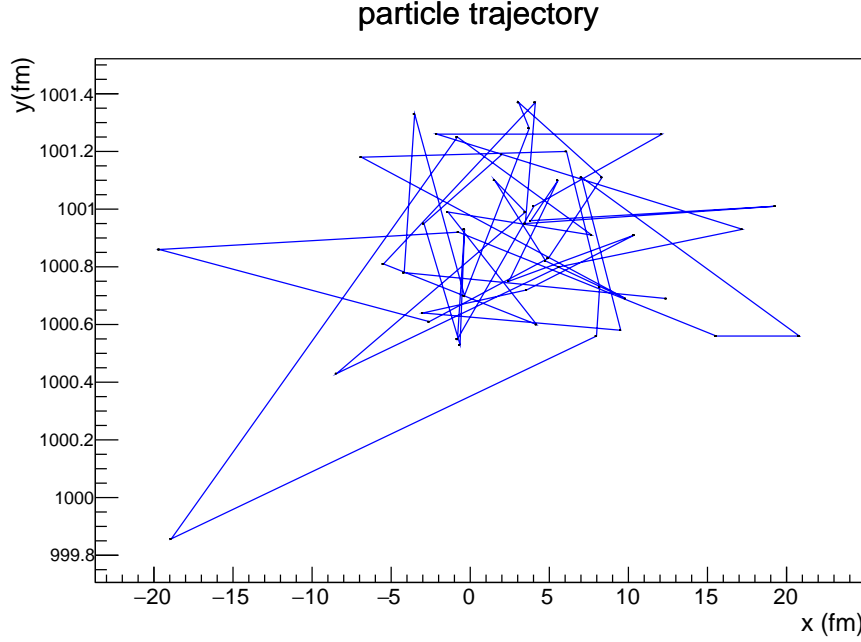


Fig. 2. Example particle trajectory of a particle with initial momentum vector $(0,0,p_z)$ with $p_z = 300$ MeV.

p_{init} [MeV]	N	μ [fm/c]	σ_t [fm/c]	χ^2/ndf
75	354.5 ± 7.2	0.144 ± 0.0023	0.102 ± 0.0015	38.56/20
80	197.1 ± 4.19	0.129 ± 0.0024	0.091 ± 0.0019	59/34
90	121.0 ± 2.5	0.104 ± 0.0018	0.074 ± 0.0008	63.02/58
100	94.0 ± 2.0	0.089 ± 0.0016	0.063 ± 0.0011	113.9/76
110	68.2 ± 1.4	0.0733 ± 0.0014	0.052 ± 0.0010	98.86/98
125	54.2 ± 1.1	0.058 ± 0.00085	0.041 ± 0.00061	188.6/158
140	21.0 ± 0.44	0.0446 ± 0.00067	0.0315 ± 0.0005	514.5/435

Table 1. Fitting results (c.f. figure 3) Gaussian fit function for different initial momenta with $R = 1.5$ fm and $N_{ch} = 1000$ charged particle and $d = 1600$ fm. Probabilities (p -values) of all fits are above 0.1%. Here N is a normalization parameter and μ is a width parameter, as indicated in the legend of figure 3. From this, the standard deviation variable σ_t results by a division by $\sqrt{2}$.

5. Results

From our simulations, we calculate the Δt difference between the expected arrival time after modification and the arrival time in the free case (ignoring the final state interaction) which appears to follow a normal distribution, as shown in fig. 3. The results of the Gaussian fits to a few example distributions are shown in table 1.

While our calculations always run until a finite distance d is reached, we are interested in the limiting case of $d \rightarrow \infty$, or a distance corresponding to actual de-

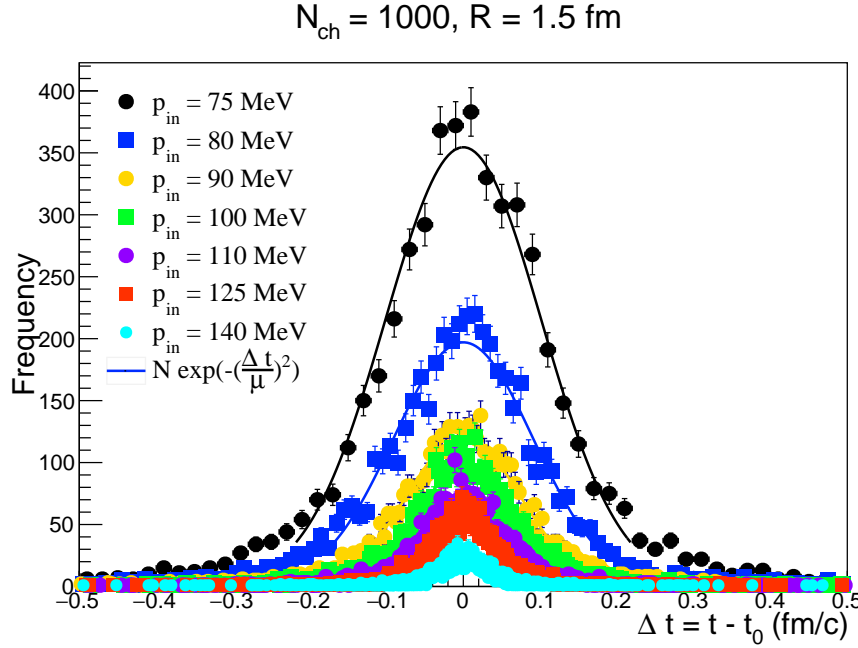


Fig. 3. Time shift distributions from the simulation for different initial momentum values.

tector sizes, practically infinity, compared to our femtometer (or up to a few hundred picometer) distances. Thus we investigate the distance-dependence of the phase-shift width, and fit it with a convergent function of the following shape:

$$\sigma_t(d) = A(1 - e^{-Bd^C}) \quad (33)$$

where A , B , and C are auxiliary parameters, and then $\sigma_t(d \rightarrow \infty) = A$. Several such example fits are shown in fig. 4. In the end we use this extrapolated width, as a function of particle momentum p , corresponding to transverse momentum p_t at or near midrapidity. The results for this extrapolated σ_t , as a function of initial particle momentum, can be seen in Fig. 5. It is clear that when the initial transverse momentum of the probe particle increases, the interactions with the cloud charge and Aharonov-Bohm effect decrease, and then the time-shift width decreases.

The time shift Δt is then connected to the phase-shift through velocity v and wavenumber k (assuming negligible change of momentum) as

$$\phi = k\Delta x = \frac{p}{\hbar}v\Delta t = \frac{p^2}{\hbar\sqrt{m^2 + p^2}}\Delta t. \quad (34)$$

Hence the width of the time-shift distribution σ_t is a good quantifier for σ the width of the phase-shift distribution:

$$\sigma = \frac{p^2}{\hbar\sqrt{m^2 + p^2}}\sigma_t. \quad (35)$$

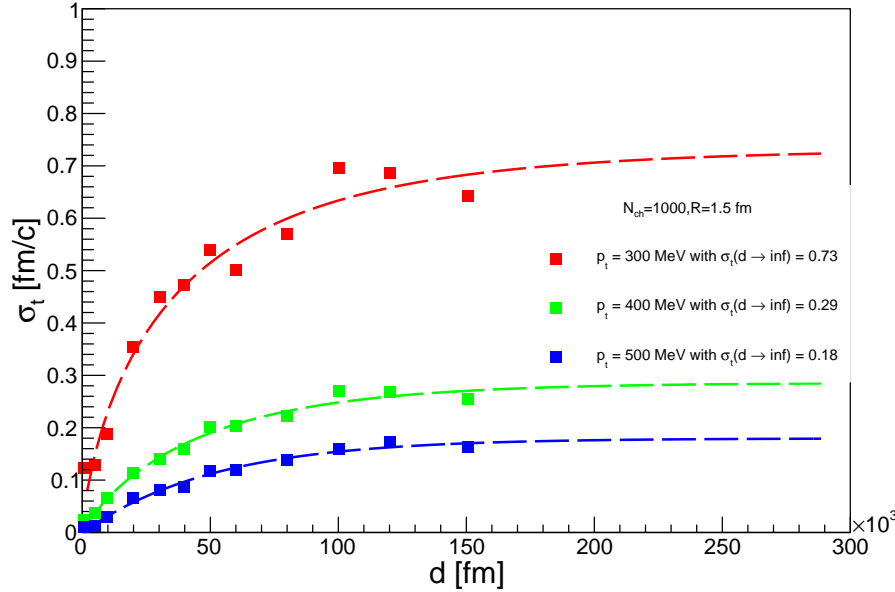


Fig. 4. The traveled distance by the investigated correlated particles with the phase-shift distribution σ_0 , for $N_{\text{ch}} = 1000$, $R = 1.5$ fm.

In this analysis, we investigated two main scenarios. The first one when $N_{\text{ch}} = 500$ particle with $R_{\text{fireball}} = 5$ (fm) and the second one when $N_{\text{ch}} = 1000$ particle with $R_{\text{fireball}} = 1.5$ fm, where N_{ch} is the number of charged particles in the charged cloud of pions, and R_{fireball} is the fireball radius of the cloud. From the second scenario ($N_{\text{ch}} = 1000$ and $R = 1.5$ fm) the intercept parameters of Bose-Einstein correlations, as shown in fig. 6, show a significant decrease for the final state effects.

If the standard deviation of the Gaussian distribution in time of flight shift σ_t can be estimated using ROOT tool, then $\sigma(p)$ may be calculated as given in equation (35). We may substitute this into

$$\lambda_2 = e^{-2\sigma^2}, \text{ and} \quad (36)$$

$$\lambda_3 = 3e^{-2\sigma^2} + 2e^{-3\sigma^2}. \quad (37)$$

The resulting parameters are shown in figs. 6 and 7. In addition, the dependence on the fireball radius charged particle multiplicity is clear from figs. 8 and 9. Finally, λ_3 is shown as a function of a density profy, $N_{\text{ch}}/R_{\text{fireball}}^3$, in fig. 10, and is found to systematically decrease with it.

6. Conclusion

The study investigates the space-time structure and inner dynamics of ultra-relativistic collisions like heavy ion collisions and pp collisions with high multiplicity

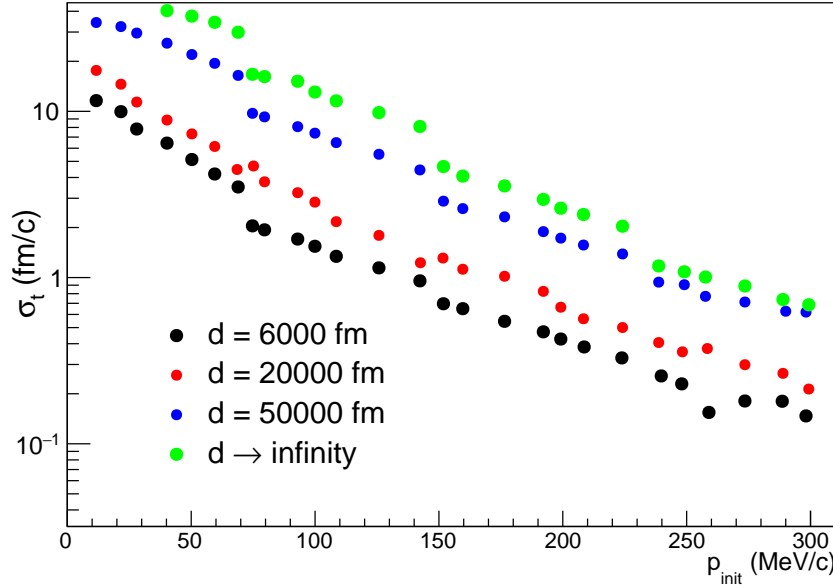


Fig. 5. The dependency of the gaussian width and then the phase shift on the initial momentum of the correlated particles.

after the freeze-out of very hot and dense matter (Quark-Gluon Plasma) using a simulation via a toy model. Changes in phases due to the Aharonov-Bohm effect, effectuated via the Coulomb interaction, may cause distortion in quantum-statistical correlations. The simulation was established from the numerical solution of the movement of particles to measure the modification of the strenght of correlation functions, via the time-shift of the arrival time. The study found that the change in phases is clear at low momenta of the investigated particle and decreases at high momenta. The study also found that this correlation strenght change depends on the charged particle density, and that for high densities this additional effect may be important to consider. This procedure would be rather resource-comsuning for state-of-the art Monte Carlo simulations of high-energy heavy-ion collisions, due to the large range of the Coulomb interaction, as well as the large timescale (hundreds of thousands of fm/c units) required for the effect to be formed. Nevertheless, when calculating momentum correlations, it can be taken into account via an afterburner, operating along the procedure outlined in this paper.

Acknowledgments

Hemida H. Mohammed would like to thank Dr. Ahmad Lotfy for his helpful discussions. This work was supported by the Hungarian NFKIH grant K-138136. M.A. Mahmoud and Hemida Hamed Mohammed were supported by Science, Technology,

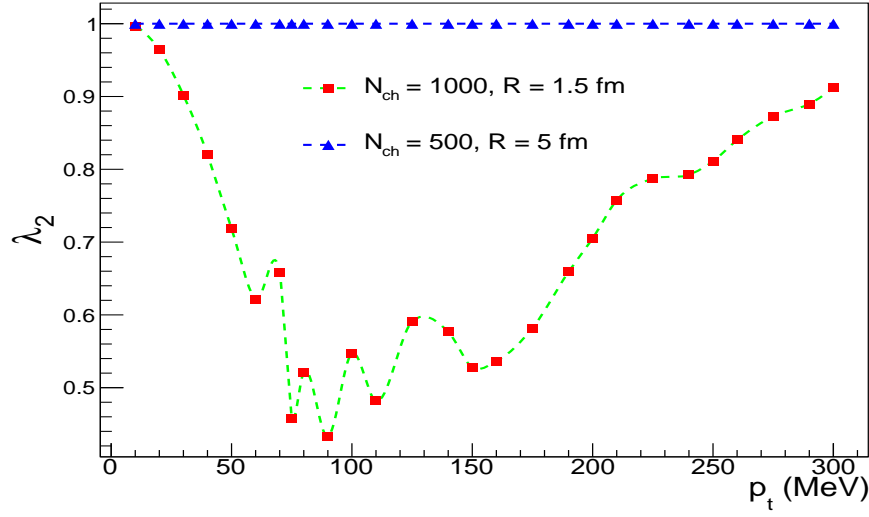


Fig. 6. The intercept parameter λ_2 as a function of the initial transverse momentum of the probe particle, for the two scenarios: $N_{ch} = 500$, $R = 5$ fm and $N_{ch} = 1000$, $R = 1.5$ fm.

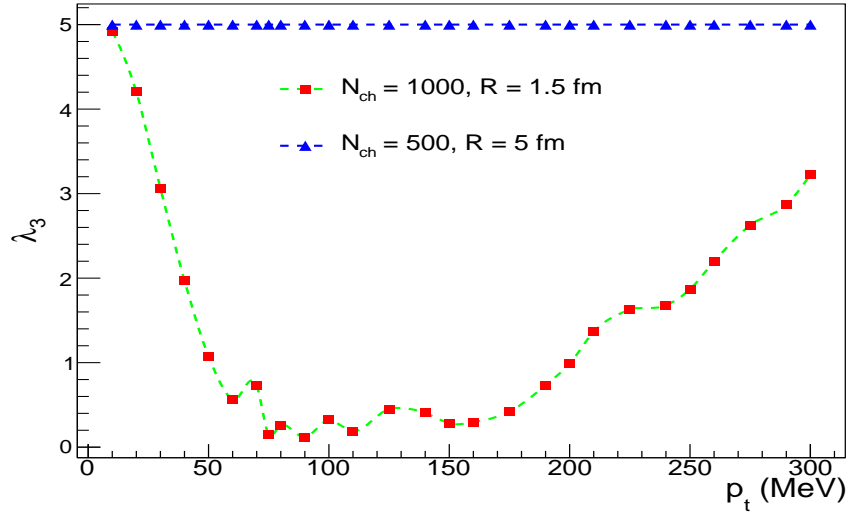


Fig. 7. The intercept parameter λ_3 as a function of the initial transverse momentum of the probe particle, for the two scenarios: $N_{ch} = 500$, $R = 5$ fm and $N_{ch} = 1000$, $R = 1.5$ fm.

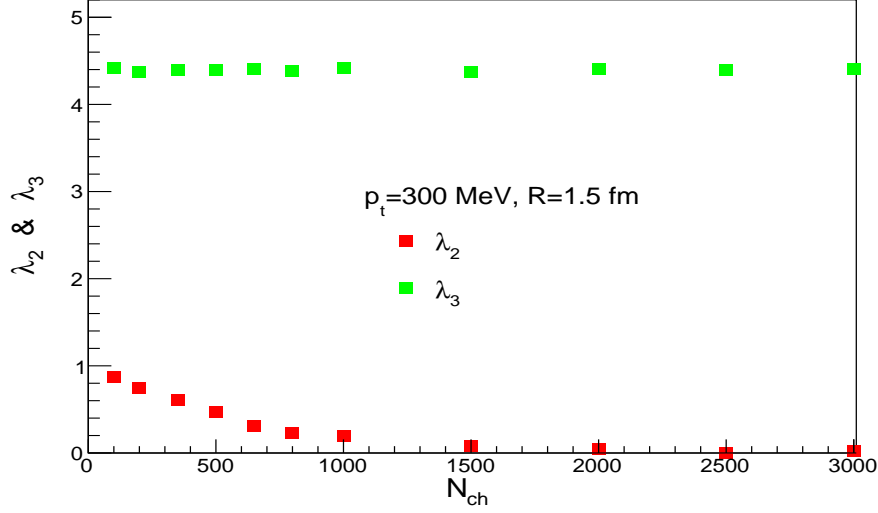


Fig. 8. Correlation strength parameters versus charged particle multiplicity.

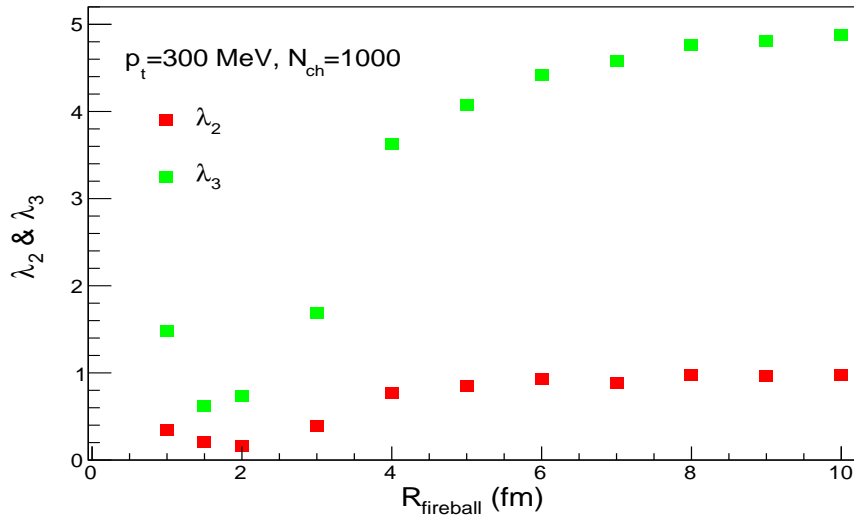


Fig. 9. Correlation strength parameters versus fireball radius.

References

1. Mike Lisa and Zbigniew Chajęcki. The multiplicity evolution of p t spectra at rhic. *Acta Physica Polonica B*, 40(4), 2009.
2. T Csörgő, B Lörstad, and J Zimányi. Bose-einstein correlations for systems with large

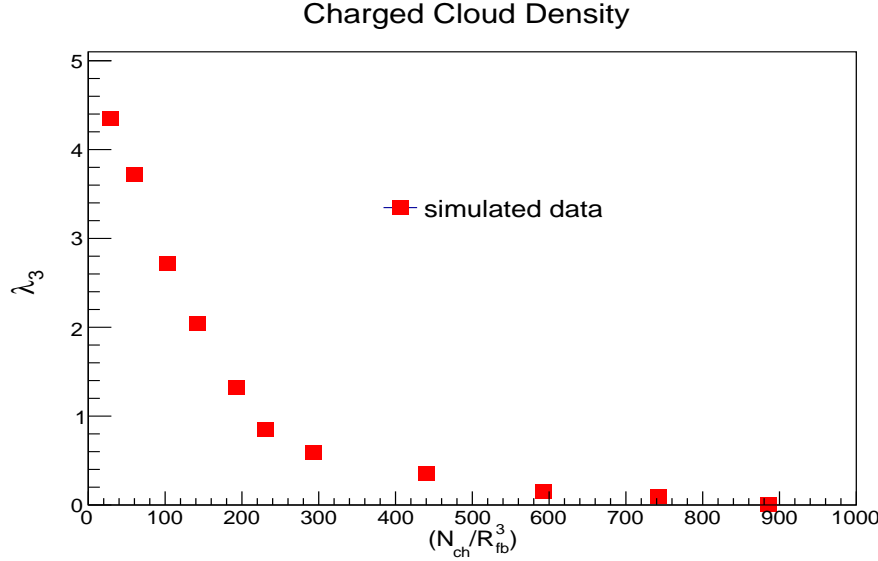


Fig. 10. Intercept parameter λ_3 versus a charged particle density proxy.

- halo. *Zeitschrift für Physik C Particles and Fields*, 71:491–497, 1996.
3. R Hanbury Brown and Richard Q Twiss. Correlation between photons in two coherent beams of light. *In: Nature*, 177:p.27, 1956.
 4. R Hanbury Brown and Richard Q Twiss. A test of a new type of stellar interferometer on sirius. *In: Nature*, 178:p.1046, 1956.
 5. MM Aggarwal, Z Ahammed, AV Alakhverdyants, I Alekseev, J Alford, BD Anderson, D Arkhipkin, GS Averichev, J Balewski, LS Barnby, et al. Pion femtoscopy in $p + p$ collisions at $s = 200$ gev. *Physical Review C—Nuclear Physics*, 83(6):064905, 2011.
 6. R Lednicky. Femtoscopy with unlike particles. *arXiv preprint nucl-th/0112011*, 2001.
 7. Michael Annan Lisa, Scott Pratt, Ron Soltz, and Urs Wiedemann. Femtoscopy in relativistic heavy ion collisions: two decades of progress. *Annu. Rev. Nucl. Part. Sci.*, 55(1):357–402, 2005.
 8. A. Adare et al. Lévy-stable two-pion Bose-Einstein correlations in $\sqrt{s_{NN}} = 200$ GeV Au+Au collisions. *Phys. Rev. C*, 97(6):064911, 2018. [Erratum: Phys.Rev.C 108, 049905 (2023)].
 9. Balázs Kórodi, Dániel Kincses, and Máté Csanád. Event-by-event investigation of the two-particle source function in sNN=2.76 TeV PbPb collisions with EPOS. *Phys. Lett. B*, 847:138295, 2023.
 10. Máté Csanád and Dániel Kincses. Femtoscopy with Lévy Sources from SPS through RHIC to LHC. *Universe*, 10(2):54, 2024.
 11. D. Kincses, M. I. Nagy, and M. Csanád. Coulomb and strong interactions in the final state of Hanbury-Brown–Twiss correlations for Lévy-type source functions. *Phys. Rev. C*, 102(6):064912, 2020.
 12. Márton Nagy, Aletta Purzsa, Máté Csanád, and Dániel Kincses. A novel method for calculating Bose–Einstein correlation functions with Coulomb final-state interaction. *Eur. Phys. J. C*, 83(11):1015, 2023.
 13. Yakir Aharonov and David Bohm. Significance of electromagnetic potentials in the

- quantum theory. *Physical review*, 115(3):485, 1959.
14. Máté Csanád, Antal Jakovác, Sándor Lökös, Ayon Mukherjee, and Srikanta Kumar Tripathy. Multi-particle quantum-statistical correlation-functions in a hubble-expanding hadron gas. In *GRIBOV-90 MEMORIAL VOLUME: FIELD THEORY, SYMMETRY, AND RELATED TOPICS Proceedings of the Memorial Workshop Devoted to the 90th Birthday of VN Gribov*, pages 261–273. World Scientific, 2021.
 15. T Csörgö. Particle interferometry from 40 mev to 40 tev. In *Particle production spanning MeV and TeV energies*, pages 203–257. Springer, 2000.
 16. R Lednický. Femtoscopic correlations and final state resonance formation. *Physics of Particles and Nuclei Letters*, 8:965–968, 2011.
 17. Yu M Sinyukov, R Lednický, SV Akkelin, Jan Pluta, and B Erazmus. Coulomb corrections for interferometry analysis of expanding hadron systems. *Physics Letters B*, 432(3-4):248–257, 1998.
 18. Radosław Maj and Stanisław Mrówczyński. Coulomb effects in femtoscopy. *Physical Review C—Nuclear Physics*, 80(3):034907, 2009.
 19. J Bolz, U Ornik, M Plümer, BR Schlei, and RM Weiner. Resonance decays and partial coherence in bose-einstein correlations. *Physical Review D*, 47(9):3860, 1993.
 20. J Kapusta, D Kharzeev, and L McLerran. Return of the prodigal goldstone boson. *Physical Review D*, 53(9):5028, 1996.
 21. Stephen E Vance, T Csörgö, and Dmitri Kharzeev. Observation of partial u a (1) restoration from two-pion bose-einstein correlations. *Physical review letters*, 81(11):2205, 1998.
 22. Yu M Sinyukov and A Yu Tolstykh. Coherence influence on the bose-einstein correlations. *Zeitschrift für Physik C Particles and Fields*, 61:593–597, 1994.
 23. Máté Csanád. Two- and three-pion Lévy femtoscopy with PHENIX. *J. Phys. Conf. Ser.*, 1070(1):012026, 2018.